Electrochemical Analysis of the Thermal Stability of 0.9-4.1 nm Diameter Gold Nanoclusters

Badri P. Mainali,[+] Dhruba K. Pattadar,[+] Jay N. Sharma and Francis P. Zamborini*

Department of Chemistry, University of Louisville, Louisville, Kentucky 40292, USA

ABSTRACT

Here we report the thermal properties of weakly-stabilized 0.9, 1.6 and 4.1 nm Au nanoparticles (NPs)/Nanoclusters (NCs) attached to indium-tin-oxide- or fluorine-doped-tin-oxide-coated glass electrodes (glass/ITO or glass/FTO). The peak oxidation potential (E_p) for Au measured by anodic stripping voltammetry (ASV) is indicative of the NP/NC size. Heating leads to a positive shift in E_p due to an increase in NP/NC size from thermal ripening. The size transition temperature (T_t) decreases with decreasing NP/NC size following the order of 4.1 nm (509 ^oC) > 1.6 nm (132 ^oC) > 0.9 nm (90 ^oC/109 ^oC, two transitions) as compared to the bulk melting point ($T_{m,b}$) for Au of 1064 ^oC. The T_t generally agrees with models describing the size-dependent melting point of Au NPs ($T_{m,NP}$) for 4.1 and 1.6 nm diameter Au NPs, but is higher than the models for 0.9 nm Au NCs. Scanning electron microscopy (SEM) and UV-Vis size analysis confirms the electrochemical results. The thermal stability of electrode-supported metal NPs/NCs is important for their effective use in catalysis, sensing, nanoelectronics, photovoltaics, and other applications.

INTRODUCTION

It is well known that the melting point of Au nanoparticles (NPs), and other metals, decreases with decreasing NP size, where the NP melting temperature ($T_{m,NP}$) relative to the bulk metal ($T_{m,B}$) is proportional to 1/diameter (1/d).[1, 2] Many thermal processes occur below T_m, such as sintering[3,

[4] and annealing,[5] (near the Tammann temperature[6]) while calcination[7] generally occurs at temperatures where polymers, surfactants, ligands, stabilizers, or additives that are in the sample become volatilized. Other thermal processes occurring on metal NPs and nanoclusters (NCs) include crystal structure transformations,[8, 9] reduction of grain boundaries and surface defects,[10] shape transformations,[5, 11] and size transformations to more stable, larger nanostructures.[12] Thermal ripening is a mechanism that may occur during annealing or sintering when a collection of NPs/NCs undergoes size transformation driven by reduction of their surface area-to-volume ratio (SA/V). Ostwald ripening[13, 14] involves the growth of larger NPs at the expense of smaller NPs through atomic diffusion from small to large NPs, whereas Smoluchowski ripening involves diffusion of entire NPs followed by coalescence and fusion of two or more NPs (also called particle diffusion-coalescence).[15, 16] Studies generally involve Au NPs and NCs that are either 1) clean (or bare) or 2) coated with various stabilizers, such as coordinating ligands (thiols, amines, phosphines),[17] surfactants,[18] polymers,[3] or ionic molecules (citrate, for example).[14]

When considering the thermal properties of Au NPs or NCs coated with stabilizers, the type of stabilizer,[19] metal size,[17] and additives[20, 21] all play a role. Depending on temperature and time, the process generally involves ligand loss, NP aggregation/sintering, and finally grain growth or coalescence.[10] Shivhare *et al.* discovered by TEM and extended X-ray absorption fine structure (EXAFS) spectroscopy that phenylethanthiolate- and hexanethiolate-coated Au_{25} NCs underwent mild sintering from 125-250 ^{o}C, where the thiol began to desorb and was eventually fully removed.[22] Smith *et al.* observed by thermogravimetric analysis (TGA), differential scanning calorimetry (DSC) and X-ray photoelectron spectroscopy (XPS) analysis that N,N,N-trimethylammonium ethanethiol trifluoroacetate-stabilized 1.2 and 0.9 nm diameter Au NCs began ligand loss (calcination) and sintering at 143 ^{o}C and 164 ^{o}C, respectively, whereas 2-

mercaptoethanesulphonic acid-stabilized 1.5 and 1.0 nm diameter Au NCs began ligand loss and sintering at 242 and 245 °C, respectively.[17] Others showed that the presence of halides greatly affected the thermal stability,[21] shape transformations occurred for ~10 nm oleylamine-coated Au NCs at 165-250 °C,[10] and 2.2 nm diameter dodecanethiol-stabilized Au NCs grew to 4.8 nm in the presence of bromide and acid at room temperature over 5 hours.[20] In these examples, understanding the size-dependent thermal properties of the clean Au NPs/NCs was not possible because the strongly-coordinated ligands and other additives played a major role as evidenced by the greater thermal stability for smaller Au NCs[17] and low thermal stability for 10 nm Au NCs in the presence of bromide.[10]

The size-dependent melting of clean Au NPs and NCs has been the subject of many studies for well over 100 years now.[23] Accordingly, there have been numerous theoretical studies modeling the size-dependent melting temperature of clean Au by (nano)thermodynamic methods,[2, 24, 25] cohesive energy calculations using different potential functions,[26, 27] Monte Carlo simulations,[28] molecular dynamics simulations,[29, 30] and bond-order-length-strength (BOLS).[31] $T_{m,NP}$ is generally related to $1/d$[31] and also depends on the specific shape (truncated octahedral, icosahedral, etc.),[32] crystal structure,[27] the support that the NP/NC is attached to,[33] the proportion of edge and corner atoms,[34] and the environment (vacuum, air, gases).[15] These different factors make it difficult to accurately predict the thermal behavior for all cases, but there have been attempts at universal melting equations.[35] The sintering of clean Au NPs/NCs depends on the initial size dispersity,[36] dispersion,[36] metal-support interaction,[37] and metal-reactant interaction,[38] showing that size is not the only important factor governing the thermal properties. Theoretical melting models agree better with experimental melting temperatures for Au NPs above 5 nm in diameter, deviating significantly for Au NCs below about 2 nm in diameter or 500 atoms.[23, 39] Most theoretical studies

compare predicted melting points to the experimental values of Buffat and Borel,[1] Dick *et al.*,[40] Sambles,[41] and Castro *et al*.[39] Common experimental techniques for measuring the melting temperature of Au NPs include microscopic,[39, 42] differential scanning calorimetry (DSC),[17] thermal gravimetric analysis (TGA),[17, 40] electron scattering,[43] and electron diffraction,[1] ranging from larger Au nanostructures that are 10s of nm down to ~2 nm diameter Au NCs.[39, 40, 42] Experimental measurements below 2 nm are rare.

In this work, we used electrochemistry to monitor the thermal properties of weakly-stabilized 0.9, 1.6 and 4.1 nm diameter Au NPs/NCs and compared the results to theory and previous experimental studies. One major advantage of our method is that the stabilizers used allowed the synthesis of Au NCs down to 0.9 nm diameter and size characterization by anodic stripping voltammetry (ASV) directly on conductive supports.[44, 45] This enabled size characterization before and after exposure to various temperatures to determine thermal stability. This is not possible with strongly-coordinated ligands, such as thiols, because they inhibit the ASV analysis and thermal properties. Our group previously used ASV for analyzing metal NP/NC size,[46] SA/V,[46] aggregation state,[47] composition and atomic arrangement,[48] and size stability under various conditions.[13, 45] Our approach allows for fast, low cost, and highly sensitive size analysis of metal NCs/NPs attached to applicable conductive support surfaces in normal environments.[49] In contrast, electron microscopy in vacuum suffers from potential electron beam effects, high cost, low sample throughput, unrealistic vacuum environment, and limited types of support surfaces. The thermal stability of metal NPs is of major scientific interest due to their unique size-dependent properties and potential applications that require their thermal stability, such as catalysis.[15]

EXPERIMENTAL

Chemicals and Materials. Sodium borohydride, (3-aminopropyl)triethoxysilane (≥ 98.0%), 2-propanol (ACS reagent) were purchased from Sigma Aldrich. Gold salt ($HAuCl_4 \cdot 3H_2O$) was synthesized from metallic Au (99.99%) in our lab. Acetone, methanol and ethyl alcohol (ACS/USP grade) were purchased from Pharmco-AAPER. Trisodium citrate salt, potassium perchlorate (99.0-100.5%), potassium bromide (GR ACS), perchloric acid (60%) and triphenyl phosphinosulfonate (TPPS, >90%) were purchased from Bio-Rad laboratories, Beantown Chemical, EMD, Merck and TCI respectively. Sodium hydroxide pellets were purchased from Fisher Scientific. Tetrakis(hydroxymethyl)phosphonium Chloride (THPC, 80% solution in water) was purchased from ACROS ORGANICS. Indium-tin-oxide (ITO)-coated and fluorine-doped tin oxide (FTO)-coated glass slides (CG-50IN-CUV, R_s = 8-12 Ω) were purchased from Delta Technologies Limited (Loveland, CO).

Synthesis of TPPS-stabilized 0.9 ± 0.2 nm Diameter Au Nanoclusters (NCs). We synthesized 0.9 ± 0.2 nm diameter Au NCs by following the protocol originally developed by Yao and co-workers and later adopted in our group.[1, 2] Briefly, 11.5 mL of a methanol solution containing a mixture of $HAuCl_4 \cdot 3H_2O$ (0.5 mmol) and TPPS sodium salt (0.75 mmol) was placed in a glass scintillation vial. Next, 3 mL of freshly prepared ice-cooled 0.2 M $NaBH_4$ solution was added under vigorous stirring. The immediate appearance of a brown color in the solution indicated the formation of 0.9 nm diameter Au NCs and the NCs were attached to electrode surfaces after stirring for 15 min.

Synthesis of THPC-stabilized 1.6 ± 0.4 nm Diameter Au NCs. We synthesized 1.6 ± 0.4 nm diameter THPC-stabilized Au NCs using the synthesis protocol reported by our group previously[3] and originally reported by Duff and co-workers.[4] Briefly, 400 μL of the reducing agent

THPC (200 μL of 80% THPC diluted to 16.66 mL of nanopure water) was added to a glass vial containing 15.5 mL of nanopure water followed by the addition of 500 μL of 0.2 M NaOH solution with constant stirring. After 2 min of stirring, 660 μL of 25 mM $HAuCl_4 \cdot 3H_2O$ was added. Immediately an orange-brown color formed in solution after the addition of $HAuCl_4 \cdot 3H_2O$, indicative of small Au NCs. These NCs were used within a couple of hours after synthesis and stable for at least 24 hours.

Synthesis of 4.1 ± 0.7 nm Average Diameter Citrate-Stabilized Au NPs. We synthesized citrate-stabilized 4.1 ± 0.7 nm average diameter Au NPs as described by our group previously[5-9] and originally reported by Murphy and co-workers.[10] In this protocol, a solution mixture of 0.5 mL of 10 mM $HAuCl_4 \cdot 3H_2O$ and 0.5 mL of 10 mM trisodium citrate was added to 18.5 mL of water followed by the addition of 0.6 mL of ice-cold 0.1 M $NaBH_4$ at once with rapid stirring for 2 hr. After the addition of $NaBH_4$, the solution color turned from colorless to orange immediately and eventually converted to a red color within 5 min, indicating the formation of Au NPs. These NPs were used for further experiments within 24 hours.

Preparation of THPC-stabilized 4.1 ± 0.7 Diameter Au NPs. We prepared THPC-coated 4.1 nm diameter Au NPs by a ligand exchange method reported recently by Gulka and coworkers.[11] Briefly, 500 μL of 100 μM THPC in water was added to 10 mL of citrate-coated 4.1 nm Au NPs synthesized by the method already described. After addition of THPC, the Au NPs immediately change from red to blue, indicating that the NPs become aggregated. The NP solution reverts back to a red color again after 24 hours, which indicates that the NPs spontaneously de-aggregate back to individual, well-separated NPs. After that, NPs were attached to glass/ITO/APTES electrodes by directly soaking the electrode in the Au NP solution. The SA/V ratio of the NPs was calculated following the method previously reported by our group to confirm that the size was ~4 nm.

Functionalization of Glass/ITO and Glass/FTO Electrodes with 3-Aminopropyltriethoxysilane (APTES) and Au NPs/NCs. Glass/ITO and glass/FTO electrodes were cleaned by sonication in acetone, ethanol, and 2-propanol for 30 min in each solvent. The glass/ITO electrode was then functionalized with APTES by immersing into a solution containing 100 µL of APTES, 10 mL of 2-propanol, and 2 to 3 drops of nanopure water and heating at 65-70^{o} C for 30 min. After 30 min, the electrode was thoroughly rinsed with 2-propanol and water and finally dried under N_2. The functionalized glass/ITO/APTES or glass/FTO/APTES was soaked into as-prepared 0.9 nm Au NCs for 10 min, 1.6 nm Au NCs (2x diluted with water) for 5 min, and 4.1 nm Au NPs (3x diluted with water) for 5 min.

Electrochemical Characterization. A CH Instruments (Austin, TX) model CHI660E electrochemical cell consisting of a 3-electrode set-up with the glass/ITO/APTES/Au NPs as the working electrode, a Pt wire counter electrode, and Ag/AgCl (3 M KCl) reference electrode were used to perform cyclic voltammetry (CV) and anodic stripping voltammetry (ASV) measurements. The CVs were scanned from -0.2 V to 1.6 V in 0.1 M $HClO_4$ at a scan rate of 0.1 V/s. The ASVs were scanned from -0.2 V to 1.4 V at a scan rate of 10 mV/s in 0.1 M $KClO_4$ plus 10 mM KBr solution. The ASV conditions were optimized for good size analysis based on the measured oxidation peak potential (E_p) as reported by our group previously.

UV-Vis Characterization. Ultraviolet-visible spectrophotometry (UV-Vis) was performed using a Varian instrument, Cary 50 Bio-spectrophotometer. UV-Vis spectra of as-prepared Au NPs were obtained in aqueous solutions of different sizes from 300-800 nm using water as the blank. For studying the effect of thermal treatment, the Au NPs were attached to glass/ITO/APTES electrodes, heated for different times and temperature, and analyzed by UV-Vis using glass/ITO/APTES as the blank.

Thermal treatment of Glass/ITO/APTES Coated with Au NPs/NCs. Glass/ITO/APTES electrodes coated with 0.9, 1.6, and 4.1 nm diameter Au NPs/NCs were heated in a Barnstead Thermolyne Furnace (Model No. FB1315M) at the temperatures and time described in the main text and SI Tables. For heating above 400 ºC, glass/FTO/APTES instead of glass/ITO/APTES electrodes were used.

Microscopic Characterization. Scanning electron microscopy (SEM) images before and after thermal treatment were obtained using a Carl Zeiss SMT AG SUPRA 35VP field emission scanning electron microscope (FE-SEM) operating at an accelerating voltage of 15.00 kV using an in-lens ion annular secondary electron detector. Transmission electron microscopy (TEM) images were obtained using a 200 kV FEI Tecnai F20 operated in TEM mode. NPs were attached to silica-coated Au TEM grids by directly soaking the APTES functionalized grid in the NP solution for 4-5 min. The grids were then rinsed with water and dried under N_2 before imaging.

RESULTS AND DISCUSSION

General Procedure. In this work, we synthesized different-sized Au NPs/NCs (0.9 ± 0.2, 1.6 ± 0.4 and 4.1 ± 0.7 nm average diameter) following the protocols reported in our previous publications (See supporting information for all experimental details).[13, 44, 46, 50] Scheme 1 shows the general procedure involved in the analysis of the thermal properties of different sized Au NPs by anodic stripping voltammetry (ASV). First, the NPs were freshly synthesized with citrate or phosphonium/phosphine stabilizers in aqueous solution (Step 1). Next, we attached the NPs to a glass/ITO/APTES electrode (Step 2). Then the NPs were thermally treated at different temperatures and times (Step 3). Finally, we analyzed the size of the Au NPs by ASV (Step 4).

ASV Analysis of Thermal Stability. We monitored the thermal stability of 0.9, 1.6 and 4.1 nm Au NPs/NCs by obtaining ASVs of the NPs/NCs attached to glass/ITO or glass/FTO electrodes after exposing them to different temperatures. Figure 1 shows the ASVs after 30 min at 25, 80, 100, 130, 150, and 200 °C for 0.9 nm and 1.6 nm Au NCs, and up to 500 °C for 4.1 nm Au NPs. The ASVs of 0.9 nm Au NCs showed a single peak with a peak potential (E_p) of 0.26 V at 25 °C. The appearance of a small second peak at 0.63 V occurred after heating at 80 °C for 30 minutes. Based on theoretical work by Plieth and our previous experimental studies,[13, 51] the peak at 0.63 V correlates to ~3.6 nm diameter Au NPs, indicating that some of the 0.9 nm Au NCs transformed into this larger size NPs by a thermal ripening mechanism. The peak current increased at 0.63 V and the peak at 0.26 V completely shifted to about 0.34 V upon heating up to 100 °C (Figure 1A). The peak at 0.34 V likely corresponds to a stable intermediate size between 0.9 nm and 1.6 nm diameter and can be considered a different size or structural transition[8] that occurs at ~90 °C. The peak at 0.34 V completely disappeared after heating to 130 °C or higher, leaving only one peak in the ASV near 0.63 V. This indicates full transformation of all Au NCs from 0.9 nm to a size between 0.9 and 1.6 nm (first transition) and finally to 3.5 – 4.0 nm diameter (second transition) due to thermal ripening. No further change occurred at 150 °C, but some broadening of the peak occurred at 200 °C, indicating the start of another size transition at higher temperature.

Scheme 1: General experimental procedure involved in this work.

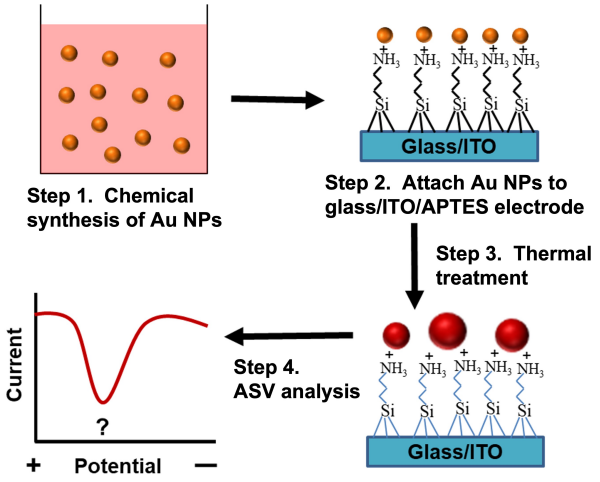

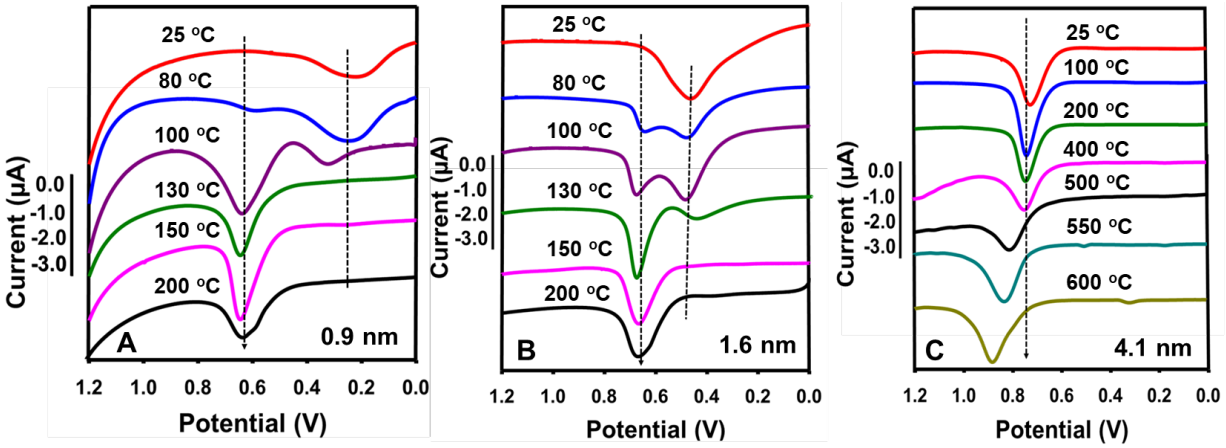

Figure 1. ASV of glass/ITO/APTES coated with 0.9 nm (A), 1.6 nm (B) and 4.1 nm (C) average diameter Au NPs before and after heating for 30 min at the indicated temperatures. ASVs were performed in 10 mM KBr plus 0.1 M $KClO_4$ solution at a scan rate of 0.010 V/s.

We observed similar behavior for 1.6 nm Au NCs when heated from room temperature to 200 °C. At 25 °C, the ASV of 1.6 nm Au NCs showed one peak at 0.47 V (Figure 1B). As the NCs were heated to 80 °C, a small shoulder peak appeared at 0.66 V, indicative of an increased size in the Au NPs. The peak current at 0.66 V gradually increased while that at 0.47 V gradually decreased with increasing temperature as occurred with 0.9 nm Au NCs (Figure 1B and Figure S1). At 130 °C, a small peak remained but it was slightly below 0.47 V. The presence of smaller Au NCs than the original size is consistent with an Ostwald Ripening process.[36] At 150 °C, one single peak appeared at 0.66 V along with complete disappearance of the original peak at 0.47 V. This indicated the complete size transformation of 1.6 nm Au NCs to ~4 nm Au NPs. Upon further heating up to 200 °C for 30 min (Figure S1), the E_p does not increase further. Some broadening of the peak occurred, indicating that another size transformation may have been starting.

In contrast to 0.9 nm and 1.6 nm Au NCs, the ASV of 4.1 nm diameter Au NPs showed one single peak with E_p at 0.71 V even after 30 min of heating up to 400 °C (Figure 1C), This is due to the greater temperature stability (higher $T_{m,NP}$) of larger Au NPs compared to smaller Au NCs.[27,

[31] Upon further heating at 500 °C for 30 min on glass/FTO, the 4.1 nm Au NPs showed an increase in peak width at half maximum indicating that some of the NPs transformed to larger sizes. After heating at 550 °C for 30 min, the E_p shifted to 0.81 V while the current at 0.71 V almost completely disappeared (Figure 1C, black plot). The 4.1 nm Au NPs started ripening at ~500 °C and transformed to >4 nm NPs (10-20 nm diameter). The E_p approached the bulk Au oxidation potential of 0.9 V after heating to 600 °C, consistent with sizes of 30 nm or larger. We could not heat the Au NPs above 600 °C due to the thermal instability of glass/FTO. Interestingly, some small peaks with lower E_p appeared in the ASVs of the 4.1 nm Au NPs after heating at 550 °C and 600 °C, which is consistent with an Ostwald Ripening process.[15, 16]

Next, we studied the effect of thermal treatment on 1.6 nm Au NCs as a function of heating time at different temperatures for up to 60 minutes by ASV. We heated the surface-attached 1.6 nm diameter Au NCs to 70 °C for up to 60 min, where the main peak sharpened, and a minor shoulder peak appeared at ~0.65 V. This is consistent with a size increase due to some thermal instability at this low temperature over longer time (Figure S1A, blue plot). After 10 min of heating at 80 °C, a clear shoulder peak at 0.65 V emerged. After 30 min, the shoulder peak emerged into a well-defined peak at ~0.68 V (Figure S1B, pink graph). The peak at ~0.68 V along with the original peak at 0.47 V indicates that some of the 1.6 nm diameter Au NCs remained stable. The peak current at 0.68 V relative to that at 0.47 V increased after 60 min of heating, consistent with more NCs transforming into bigger sizes with time (Figure S1B, black graph). Figure S1C shows ASVs following the heating of glass/ITO/APTES/Au NPs (1.6 nm) at 100 °C for 10, 30 and 60 min. After 10 and 30 min, peaks exist at 0.47 and 0.68 V (blue and pink plots), where the peak at 0.47 V sharpened. After 60 min of heating, the peak at 0.68 V became dominant but not all Au NCs transformed in size (black plot). Heating at 130 °C led to an even more dominant peak at

0.68 V (Figure S1D) until the peak at 0.47 V completely disappeared at 150 °C after 30 and 60 min (Figure S1E), indicating complete thermal size transformation of the 1.6 nm Au NCs. Figure S1F shows ASVs of 1.6 nm Au NCs attached to glass/ITO/APTES following heat treatment for 60 minutes at temperatures up to 400 °C. Complete size transformation occurred at 200 °C and there were very small changes from 200-400 °C. The peak broadened at 400 °C with a minor positive shift in E_p. The thermal ripening that occurred at 200-300 °C led to larger-sized NPs that were fairly stable up to at least 400 °C.

Microscopy and Spectroscopy Analysis of Thermal Stability. Scanning electron microscopy (SEM) images and UV-vis spectra of the Au NPs before and after heating at various temperatures and time are consistent with the ASV data. Figure S2 shows that the 1.6 nm Au NCs were not visible by SEM before heating (Figure S2A) but became visible (Figure S2B) with a diameter of 5.7 ± 0.9 nm when heated at 400 °C for 60 min (Figure S2C), consistent with the ASV in Figure S1F. The SEM images of citrate-coated 4.1 nm Au NPs before (Figure S2D) and after thermal treatment at 200 and 400 °C (Figure S2E-F) showed no significant change in size after heating. This is generally consistent with the ASV, although ASV showed a small shift and broadening of the peak (Figure 1C). The ASV may be potentially more sensitive than SEM at this size. We monitored the effect of heating 1.6 nm Au NCs attached to glass/ITO/APTES by UV-Vis spectroscopy. Figure S3 shows a featureless spectrum for the 1.6 nm Au NCs characteristic of light scattering by the sub 2 nm diameter Au NCs, where there is no localized surface plasmon resonance (LSPR) absorbance peak. After heating from 100 °C up to 400 °C, a LSPR peak developed in the 500-550 nm region, consistent with NCs above 2 nm in diameter. The peak increased and red shifted as the temperature increased, indicative of larger size NPs or aggregates, consistent with the ASV and SEM data on thermal ripening.

Size Transition Temperature (T_t) and Theoretical Melting Point ($T_{m,NP}$). We next used the ASV data to quantify the size transition temperature (T_t) for the different sized Au NPs as they transform from their original size to a more stable larger size upon heating. This can be determined from ASV since the E_p starts at one value, indicative of the NP/NC size, and then shifts to a more positive value upon heating due to size transformation to a larger size. We plotted the ratio of the current from the final transformed peak ($i_{p,f}$) to the current from the inital peak ($i_{p,i}$) as a function of temperature for the different sized Au NPs/NCs (Tables S1 and S2). For example, the E_p shifts from 0.26 V to 0.63 V for the 0.9 nm diameter Au NCs, which correlates to a size transformation from 0.9 nm diameter to ~3.6 nm diameter NPs. A plot of $i_{p,f}/i_{p,i}$, or $i_{0.63V}/i_{0.26V}$, as a function of temperature produced a sigmoidal curve, where T_t is defined as the inflection point. For this analysis, we ignored the transition from E_p = 0.26 to E_p = 0.34 V for 0.9 nm Au NCs since we only had one data point there, but we approximate T_t for that first transition is ~90 ^oC. The same plot was generated for 1.6 nm Au NCs and 4.1 nm Au NPs using the ratios of $i_{0.66V}/i_{0.47V}$ and $i_{0.80V}/i_{0.72V}$, respectively, versus temperature as shown in Figure 2A. The transition is from 1.6 nm to 3.5-4.0 nm and 4.1 nm to 15-20 nm diameter, respectively. We fit the sigmoidal plots for 0.9, 1.6 and 4.1 nm Au NCs/NPs in Figure 2A to the Boltzmann function and took a normalized first derivative as shown in Figure 2B. T_t is the peak temperature in the first derivative plot. The T_t values are 90/109 ^oC, 132 ^oC, and 509 ^oC for 0.9 nm (red plot), 1.6 nm (black plot), and 4.1 nm (blue plot) Au NPs/NCs, respectively. Figure 2C compares our experimental T_t values to thermodynamic models of size-dependent $T_{m,NP}$ for Au NPs based on size and shape,[25] nanothermodynamics,[24] liquid drop model (LDM),[52] homogenous growth (HOG),[31] liquid nucleation and growth (LNG),[31] and liquid shell model (LSM).[31] The experimental values agree best with LDM[52] and the

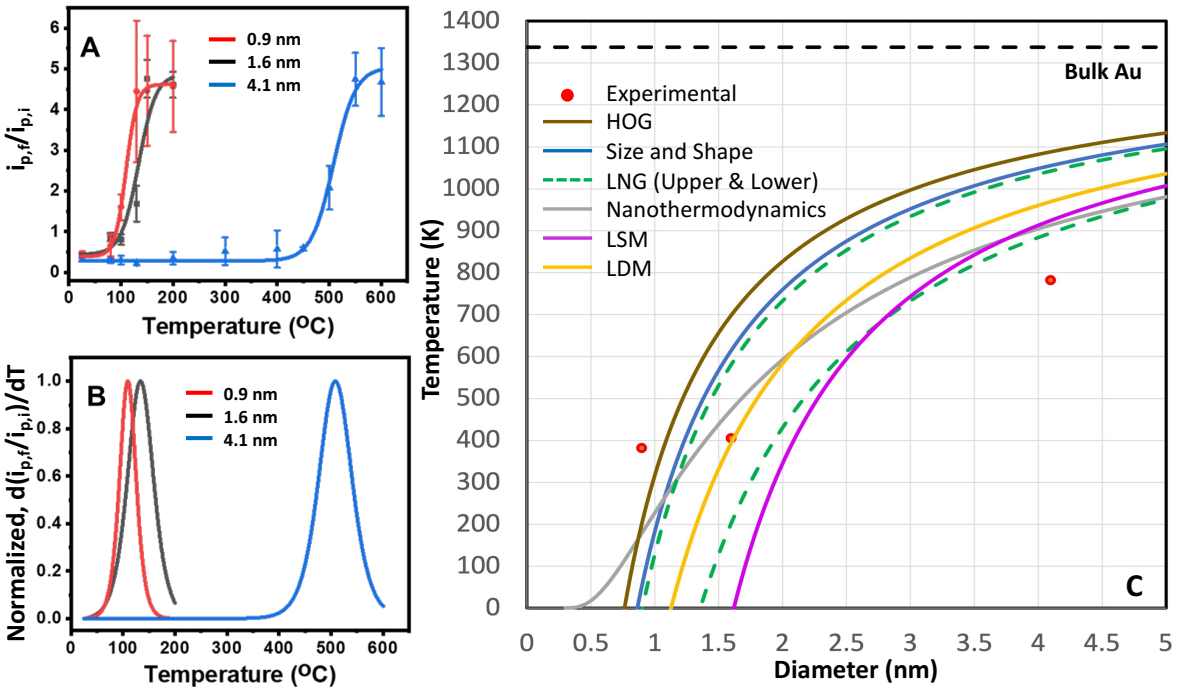

Figure 2. Plot of ratio of peak current at higher potential ($i_{p,f}$) to lower potential ($i_{p,i}$) for 0.9 nm ($i_{0.63V}/i_{0.26V}$), 1.6 nm ($i_{0.66V}/i_{0.47V}$), and 4.1 nm ($i_{0.80V}/i_{0.72V}$) diameter Au NPs heated for 30 min at different temperatures (A), plot of first order derivative of the normalized peak current ratios from A as a function temperature (B), and a plot of the experimental transition temperatures (converted to K) from frame B as a function of Au NP radius compared to the bulk melting point of Au and theoretical melting point of Au NPs as a function of diameter calculated by several different models in the literature as described in the text (C).

nanothermodynamics[25] models for the 4.1 and 1.6 nm Au NCs, but T_t is larger than expected for the 0.9 nm Au NCs for all models.

One potential issue with our size-dependent thermal studies is that the 4.1 nm diameter Au NPs are stabilized by citrate while the 0.9 nm and 1.6 nm diameter Au NCs are stabilized by THPC and TPPS, respectively. To rule out the ligands as the main reason for the different thermal properties, we compared ASV and SA/V data at different temperatures for citrate- and THPC-stabilized 4.1 nm diameter Au NPs following the work of Sharma *et al.*[46] to determine their size at different temperatures. The ASV peak of the THPC-stabilized 4.1 nm Au NPs was slightly broader and had a small positive shift in E_p (Figure S4) along with smaller SA/V ratios (Table S3) compared to the

citrate-stabilized 4.1 nm Au NPs due to increased Au NP diameter, but the slightly lower stability with THPC was not significant enough to explain the large differences between 0.9 nm/1.6 nm Au NCs and the 4.1 nm Au NPs. Exploring the role of different ligands and additives on the size-dependent thermal properties by ASV will be the focus of a future study.

Comparison to Literature. Previous melting and sintering studies involved Au NPs/NCs coated with various stabilizers or those that had clean Au surfaces. Within these classes there are also unsupported and supported Au NPs/NCs, where the supported ones can be close-packed assemblies, well-separated assemblies, or individual NPs/NCs. We do not compare our work to Au NCs stabilized with strongly-coordinated ligands, such as thiols, since we have well separated, electrode-supported Au NPs/NCs with weak ligand stabilizers that do not significantly alter the physical properties of the Au based on the expected decreasing E_p values and decreasing thermal stability with decreasing size.[44, 45, 49] Accordingly, we compare our work to experimental and theoretical studies of clean Au NCs in the literature. As shown in Figure 2C, our T_t values are generally in the expected range when comparing to theoretical $T_{m,NP}$ values based on thermodynamic calculations of clean, unsupported Au NPs/NCs (see also Figure S5). Table S4 shows the expected $T_{m,NP}$ for the same size Au NPs we studied using these thermodynamic models and different molecular dynamics (MD) simulations. The experimental T_t value for 4.1 nm Au NPs is a little lower than expected and that for 0.9 nm diameter Au NCs is higher than expected. Our results match best the $T_{m,NP}$ for 4.1 nm and 1.6 nm diameter Au NPs/NCs calculated using the nanothermodynamics[25] and LDM[52] models. All thermodynamic models fail for 0.9 nm Au NCs and some also fail for 1.6 nm Au NCs. The calculated $T_{m,NP}$ values from MD simulations for 4.1 nm (630-760 ^{o}C) and 1.6 nm (230-350 ^{o}C) Au NPs/NCs are 100-200 ^{o}C larger than our experimental values. MD calculations for smaller clusters below 1.0 nm vary. The calculations

for Au_{13} by Garzon *et al.*[53] and Rey *et al.*[54] are 128 °C and 140 °C, respectively, which is very close to our T_t value for 0.9 nm Au NCs. In contrast, MD calculations by Soulé de Bas on Au_7, Au_{13}, and Au_{20} predict higher thermal stability for these clusters, near the $T_{m,b}$ and even above $T_{m,b}$ for the Au_7 cluster.[55] Breakdowns in thermodynamic models are expected for NCs below about 500 atoms or 2.0 nm.[37, 39]

Table S5 compares our T_t values to experimental $T_{m,NP}$ values. Our values for 1.6 nm and 4.1 nm Au NPs are lower than experimental values measured in the literature other than the $T_{m,NP}$ of 47 °C reported by Buffat and Borel[1] for 2.5 nm Au NCs using electron diffraction following a correction based on theory. The uncorrected data showed a $T_{m,NP}$ near 400 °C, which is more in line with other reports and theory. Castro *et al.* reported a $T_{m,NP}$ of 315 °C for an individual 1.2 nm diameter Au NC on a tungsten tip using field emission microscopy (FEM).[39] While this is larger than our value, it is interesting that a slightly larger Au NC of 2.3 nm diameter had a lower $T_{m,NP}$ of 260 °C and that the $T_{m,NP}$ for clusters below about 2.5 nm diameter all had similar values.[37, 39] This is consistent with our 0.9 nm $T_{m,NP}$ being close to 1.6 nm, except our values are lower. Clearly more experiments and theory are needed for $T_{m,NP}$ of metal NCs < 2 nm.

It is likely that our T_t measurement reflects the temperature for thermal sintering or ripening and is lower than the true $T_{m,NP}$ (solid to liquid transition).[6] The Hüttig and Tammann temperatures for Au are 401 K (128 °C) and 668 K (395 °C), respectively.[6] At the Hüttig temperature (~$0.3T_{m,b}$), atoms at defects become mobile, where atoms in the bulk become mobile at the Tammann temperature (~$0.5T_{m,b}$).[6] We expect the Hüttig and Tammann temperatures to be size-dependent and the $T_{m,NP}$ may even be the same as the Hüttig temperature for Au NCs that contain mostly surface defect atoms, such as the Au_{13} NC, where 12 out of 13 atoms are at the surface (Garzon *et al.* calculated the $T_{m,NP}$ to be $0.3T_{m,b}$ for Au_{13}).[53] A review of the literature shows experimental

and theoretical examples of both particle diffusion-coalescence ripening (Smoluchowski Ripening) and atom migration ripening (Ostwald Ripening) for Au NPs/NCs of our sizes below the calculated $T_{m,NP}$. For example, Reich *et al.* observed 4 nm average diameter Au NPs undergoing Ostwald ripening at temperatures ranging from 390 ºC up to 550 ºC, which is similar to our T_t for 4.1 nm Au NPs.[56] Hu *et al*. observed Smoluchowski ripening for clean 3.4-4.4 nm Au NPs on amorphous carbon at 250 ºC in oxygen for 2 hours.[15] Size-selected Au_4, Au_6, Au_{13}, and Au_{20} NCs deposited onto amorphous carbon grew in size at room temperature by Ostwald ripening over a several month time period, where the Au atom diffusion and ripening kinetics were greater for the larger Au NCs.[57] Nelli *et al.*[58] modeled the ripening by coalescence for 1.6 nm diameter Au_{147} NCs occurring at 127-227 ºC and Wan *et al.*[59] calculated the onset for Ostwald Ripening at 327 ºC for 1 nm diameter Au NCs on TiO_2(110). Triphenylphosphine (TPP)-stabilized Au_{11} NCs on a mesoporous silica support increased in size from 0.8 nm to 1.9 nm at 200 ºC over 16 hours by cluster migration and aggregation.[7, 60] While Ostwald ripening[36, 37] and NP coalescence-based Smoluchowski ripening depend on many different factors, both processes can occur in ambient conditions at temperatures well below the $T_{m,NP}$ and are important to consider.

CONCLUSIONS

We characterized the thermal properties of weakly-stabilized 0.9 nm, 1.6 nm, and 4.1 nm diameter Au NCs/NPs using ASV. A decrease in thermal stability with decreasing Au NC size shows that the weak stabilizers do not strongly alter the size-dependent thermal properties of the Au, which allows us to assess the properties of the metal without dominant ligand-metal interactions. The onset for size ripening of TPPS 0.9 nm, THPC 1.6 nm, and citrate 4.1 nm Au occurred at ~70 ºC, 70-80 ºC, and 400 ºC, respectively. The 0.9 nm Au NCs exhibited two T_t

points at 90 and 109 °C while the T_t of 1.6 nm and 4.1 nm was 132 °C and 509 °C, respectively. The ASV data was consistent with the appearance of a LSPR band in the UV-Vis spectrum and selected size analysis by SEM with temperature. The thermal stability is generally consistent with melting point depression and ripening models observed previously in the literature. Some thermodynamic models predict 4.1 nm and 1.6 nm Au NPs/NCs well, but there is a clear breakdown for the 0.9 nm Au NCs, as it has much greater thermal stability than expected by thermodynamics. The lower than expected thermal stability for 1.6 nm and 4.1 nm Au NPs is likely due to the fact that ASV measures the sintering/ripening temperature, which occurs lower than the $T_{m,NP.}$ Our results on 0.9 nm Au NCs is most consistent with the MD simulations of Garzon *et al.*[53] placing the $T_{m,NP}$ at about $0.3T_{m,b}$. It is also qualitatively consistent with the experimental results of Castro *et al.*, who showed similar thermal behavior for Au NCs below about 2.5 nm.[39] More work will be needed to improve theoretical models in this size range, while ASV can clearly find great use to determine the experimental temperature for size transformation/melting as a function of NP/NC size, support surface, ligand stabilizer, and metallic composition. ASV analysis is high throughput, low cost, and highly sensitive to size. The thermal properties of sub-1 nm NCs are very difficult to analyze under real conditions attached to normal electrode supports using other methods.

Supporting Information

Details of the experimental procedures, ASV of 1.6 nm Au NCs heated for different time and temperature, SEM images of 1.6 and 4.1 nm Au NPs on glass/ITO/APTES after heating at different temperatures, UV-vis spectra of Au NCs before and after heating at different temperatures, ASV of 4.1 nm citate- and THPC-coated Au NPs upon heating, and plot of theoretical melting point of

Au NPs as a function of diameter for several different thermodynamic models up to 30 nm diameter with our experimental data plotted for comparison are provided in Figures S1 through S5, respectively. Individual peak currents for electrooxidation of Au NCs/NPs from ASV at two different potentials upon 30 min heating at different temperatures are provided in Tables S1 and S2. Integrated Au oxidation charge under the peaks in CV and ASV, calculated SA/V ratios, and calculated NP size for 4.1 nm citrate-coated Au NPs after ligand exchange with THPC and heating are provided in Table S3. Comparisons of our T_t values to theoretical melting points and experimental melting points in the literature for the same sizes are provided in Table S4 and S5, respectively.

AUTHOR INFORMATION

Corresponding Author

*E-mail: f.zamborini@louisville.edu

Author Contributions

+ B.P.M. and D.K.P. contributed equally.

Notes

The authors declare no competing financial interest.

ACKNOWLEDGMENTS

We gratefully acknowledge the National Science Foundation (NSF) for financial support of this research through grants CHE-1611170 and CHE-2004169.

REFERENCES

(1) Buffat, P.; Borel, J.-P. Size Effect on the Melting Temperature of Gold Partlcles. **1976**.
(2) Guisbiers, G. Advances in Thermodynamic Modelling of Nanoparticles. *Adv. Phys.* **2019**, *4*, 1668299.
(3) Behafarid, F.; Cuenya, B. R. Towards the Understanding of Sintering Phenomena at the Nanoscale: Geometric and Environmental Effects. *Top. Catal.* **2013**, *56*, 1542-1559.
(4) Samsonov, V. M.; Talyzin, I. V.; Puytov, V. V.; Vasilyev, S. A.; Romanov, A. A.; Alymov, M. I. When Mechanisms of Coalescence and Sintering at the Nanoscale Fundamentally Differ: Molecular Dynamics Study. *J. Chem. Phys.* **2022**, *156*, 214302.
(5) Tan, B. J. Y.; Sow, C. H.; Koh, T. S.; Chin, K. C.; Wee, A. T. S.; Ong, C. K. Fabrication of Size-Tunable Gold Nanoparticles Array with Nanosphere Lithography, Reactive Ion Etching, and Thermal Annealing. *J. Phys. Chem. B* **2005**, *109*, 11100-11109.
(6) Moulijn, J. A.; van Diepen, A. E.; Kapteijn, F. Catalyst Deactivation: Is it predictable? What to Do? *Appl. Catal. A-Gen.* **2001**, *212*, 3–16.
(7) Liu, Y.; Tsunoyama, H.; Akita, T.; Tsukuda, T. Preparation of ∼1 nm Gold Clusters Confined Within Mesoporous Silica and Microwave-Assisted Catalytic Application for Alcohol Oxidation. *J. Phys. Chem. C Lett.* **2009**, *113*, 13457–13461.
(8) Smith, D. J.; Petford-Long, A. K.; Wallenberg, L. R.; Bovin, J.-O. Dynamic Atomic-Level Rearrangements in Small Gold Particles. *Science* **1986**, *233*, 872-875.
(9) Koga, K.; Ikeshoji, T.; Sugawara, K. Size- and Temperature-Dependent Structural Transitions in Gold Nanoparticles. *Phys. Rev. Lett.* **2004**, *92*, 115507.
(10) Ingham, B.; Lim, T. H.; Dotzler, C. J.; Henning, A.; Toney, M. F.; Tilley, R. D. How Nanoparticles Coalesce: An in Situ Study of Au Nanoparticle Aggregation and Grain Growth. *Chem. Mater.* **2011**, *23*, 3312–3317.
(11) Wang, Y. Q.; Liang, W. S.; Geng, C. Y. Shape Evolution of Gold Nanoparticles. *J. Nanopart. Res.* **2010**, *12*, 655–661.
(12) Bore, M. T.; Pham, H. N.; Switzer, E. E.; Ward, T. L.; Fukuoka, A.; Datye, A. K. The Role of Pore Size and Structure on the Thermal Stability of Gold Nanoparticles within Mesoporous Silica. *J. Phys. Chem. B* **2005**, *109*, 2873-2880.
(13) Mainali, B. P.; Pattadar, D. K.; Zamborini, F. P. Size-Dependent Ripening of Gold Nanoparticles Through Repetitive Electrochemical Surface Oxidation-Reduction Cycling. *J. Electrochem. Soc.* **2020**, *167*, 146503-146511.
(14) Pattadar, D. K.; Zamborini, F. P. Effect of Size, Coverage, and Dispersity on the Potential-Controlled Ostwald Ripening of Metal Nanoparticles. *Langmuir,* **2019**, *35*, 16416−16426.
(15) Hu, K.-J.; Plant, S. R.; Ellis, P. R.; Brown, C. M.; Bishop, P. T.; Palmer, R. E. Atomic Resolution Observation of a Size-Dependent Change in the Ripening Modes of Mass-Selected Au Nanoclusters Involved in CO Oxidation. *J. Am. Chem. Soc.* **2015**, *137*, 15161−15168.
(16) Hansen, T. W.; Delariva, A. T.; Challa, S. R.; Datye, A. K. Sintering of Catalytic Nanoparticles: Particle Migration or Ostwald Ripening? *Acc. Chem. Res.* **2013**, *46*, 1720-1730.
(17) Smith, B. L.; Hutchison, J. E. Transformations During Sintering of Small (Dcore < 2 nm) Ligand-stabilized Gold Nanoparticles: Influence of Ligand Functionality and Core Size. *J. Phy. Chem. C* **2013**, *117*, 25127-25137.
(18) Albrecht, W.; van de Glind, A.; Yoshida, H.; Isozaki, Y.; Imhof, A.; van Blaaderen, A.; de Jongh, P. E.; de Jong, K. P.; Zečević, J.; Takeda, S. Impact of the Electron Beam on the Thermal Stability of Gold Nanorods Studied by /Environmental Transmission Electron Microscopy. *Ultramicroscopy* **2018**, *193*, 97-103.
(19) King, S. R.; Shimmon, S.; Totonjian, D. D.; McDonagh, A. M. Influence of Bound versus Non-Bound Stabilizing Molecules on the Thermal Stability of Gold Nanoparticles. *J. Phys. Chem. C* **2017**, *121*, 13944−13951.
(20) Kanehara, M.; Sakurai, J.; Sugimura, H.; Teranishi, T. Room-Temperature Size Evolution of Thiol-Protected Gold Nanoparticles Assisted by Proton Acids and Halogen Anions. *J. Am. Chem. Soc.* **2009**, *131*, 1630–1631.

(21) Yu, Y.; Goodfellow, B. W.; Rasch, M. R.; Bosoy, C.; Smilgies, D.-M.; Korgel, B. A. Role of Halides in the Ordered Structure Transitions of Heated Gold Nanocrystal Superlattices. *Langmuir* **2015**, *31*, 6924−6932.
(22) Shivhare, A.; Chevrier, D. M.; Purves, R. W.; Scott, R. W. J. Following the Thermal Activation of Au25(SR)18 Clusters for Catalysis by X-ray Absorption Spectroscopy. *J. Phys. Chem. C* **2013**, *117*, 20007-20016.
(23) Nanda, K. K. Size-dependent Melting of Nanoparticles: Hundred Years of Thermodynamic Model. *Pramana* **2009**, *72*, 617-628.
(24) Yang, C. C.; Mai, Y.-W. Thermodynamics at the Nanoscale: A New Approach to the Investigation of Unique Physicochemical Properties of Nanomaterials. *Mater. Sci. Eng. R* **2014**, *79*, 1–40.
(25) Qi, W. H.; Wang, M. P. Size and Shape Dependent Melting Temperature of Metallic Nanoparticles. *Mater. Chem. Phys.* **2004**, *88*, 280–284.
(26) Aldossary, O. M.; Rsheed, A. A. A New Generalized Morse Potential Function for Calculating Cohesive Energy of Nanoparticles. *Energies* **2020**, *13*, 3323.
(27) Rsheed, A. A.; Aldawood, S.; Aldossary, O. M. The Size and Shape Effects on the Melting Point of Nanoparticles Based on the Lennard-Jones Potential Function. *Nanomaterials* **2021**, *11*, 2916.
(28) Wanner, M.; Werner, R.; Gerthsen, D. Dynamics of Gold Clusters on Amorphous Carbon Films Induced by Annealing in a Transmission Electron Microscope. *Surf. Sci.* **2006**, *600*, 632–640.
(29) Shim, J.-H.; Lee, B.-J.; Cho, Y. W. Thermal Stability of Unsupported Gold Nanoparticle: A Molecular Dynamics Study. *Surf. Sci.* **2002**, *512*, 262–268.
(30) Shibuta, Y.; Suzuki, T. Melting and Solidification Point of FCC-Metal Nanoparticles with Respect to Particle Size: A Molecular Dynamics Study. *Chem. Phys. Lett.* **2010**, *498*, 323–327.
(31) Guenther, G.; Guillon, O. Models of Size-dependent Nanoparticle Melting Tested on Gold. *J. Mater. Sci.* **2014**, *49*, 7915-7932.
(32) Zhu, J.; Fu, Q.; Xue, Y.; Cui, Z. Accurate Thermodynamic Relations of the Melting Temperature of Nanocrystals with Different Shapes and Pure Theoretical Calculation. *Mater. Chem. Phys.* **2017**, *192*, 22-28.
(33) Luo, W.; Su, K.; Li, K.; Liao, G.; Hu, N.; Jia, M. Substrate Effect on the Melting Temperature of Gold Nanoparticles. *J. Chem. Phys.* **2012**, *136*, 234704.
(34) Shidpour, R.; H, H. D.; Vossoughi, M. Analytical Model Based on Cohesive Energy to Indicate the Edge and Corner Effects on Melting Temperature of Metallic Nanoparticles. *Chem. Phys.* **2010**, *378*, 14–18.
(35) Xiong, S.; Qi, W.; Cheng, Y.; Huang, B.; Wangab, M.; Lia, Y. Universal Relation for Size Dependent Thermodynamic Properties of Metallic Nanoparticles. *Phys. Chem. Chem. Phys* **2011**, *13*, 10652–10660.
(36) Hu, S.; Li, W.-X. Influence of Particle Size Distribution on Lifetime and Thermal Stability of Ostwald Ripening of Supported Particles. *ChemCatChem* **2018**, *10*, 2900 – 2907.
(37) Hu, S.; Li, W.-X. Theoretical Investigation of Metal-Support Interactions on Ripening Kinetics of Supported Particles. *ChemNanoMat* **2018**, *4*, 510 –517.
(38) Hu, S.; Ouyang, R.; Li, W.-X. First-principles Kinetics Study of Carbon Monoxide Promoted Ostwald Ripening of Au Particles on FeO/Pt(111). *J. Energy Chem.* **2019**, *30*, 108–113.
(39) Castro, T.; Reifenberger, R.; Choi, E.; Andres, R. P. Size-dependent Melting Temperature of Individual Nanometer-sized Metallic Clusters. *Phys. Rev. B* **1990**, *42*, 8548-8556.
(40) Dick, K.; Dhanasekaran, T.; Zhang, Z.; Meisel, D. Size-Dependent Melting of Silica-Encapsulated Gold Nanoparticles. *J. Am. Chem. Soc.* **2002**, *124*, 2312-2317.
(41) Sambles, J. R. An Electron Microscope Study of Evaporating Gold Particles: The Kelvin Equation for Liquid Gold and the Lowering of the Melting Point of Solid Gold Particles. *Proc. R. Soc. Lond. A* **1971**, *324*, 339-351.
(42) Schlexer, P.; Andersen, A. B.; Sebok, B.; Chorkendorff, I.; Schiøtz, J.; Hansen, T. W. Size-Dependence of the Melting Temperature of Individual Au Nanoparticles. *Part. Part. Syst. Charact.* **2019**, *36*, 1800480-1800487.

(43) Borisyuk, P. V.; Borman, V. D.; Krasovskii, P. A.; Pushkin, M. A.; Tronin, V. N.; Troyan, V. I. Method for Measuring the Melting Temperature of Gold Nanoclusters on Substrate Surfaces. *Meas. Tech.* **2010**, *53*, 128-133.
(44) Pattadar, D. K.; Mainali, B. P.; Jasinski, J. B.; Zamborini, F. P. Electrooxidation, Size Stability, and Electrocatalytic Activity of 0.9 nm Diameter Gold Nanoclusters Coated with a Weak Stabilizer. *ChemElectroChem* **2020**, *7*, 800-809.
(45) Pattadar, D. K.; Zamborini, F. P. Size Stability Study of Catalytically Active Sub-2 nm Diameter Gold Nanoparticles Synthesized with Weak Stabilizers. *J. Am. Chem. Soc.* **2018**, *140*, 14126-14133.
(46) Sharma, J. N.; Pattadar, D. K.; Mainali, B. P.; Zamborini, F. P. Size Determination of Metal Nanoparticles Based on Electrochemically Measured Surface-Area-to-Volume Ratios. *Anal. Chem.* **2018**, *90*, 9308-9314.
(47) Allen, S. L.; Sharma, J. N.; Zamborini, F. P. Aggregation-Dependent Oxidation of Metal Nanoparticles. *J. Am. Chem. Soc.* **2017**, *139*, 12895-12898.
(48) Pattadar, D. K.; Zamborini, F. P. Halide-Dependent Dealloying of Cux/Auy Core/Shell Nanoparticles for Composition Analysis by Anodic Stripping Voltammetry. *J. Phys. Chem. C* **2019**, *123*, 9496-9505.
(49) Pattadar, D. K.; Sharma, J. N.; Mainali, B. P.; Zamborini, F. P. Anodic Stripping Electrochemical Analysis of Metal Nanoparticles. *Curr. Opi. Electrochem.* **2019**, *13*, 147-156.
(50) Mainali, B. P.; Pattadar, D. K.; Zamborini, F. P. Reverse Size-Dependent Electrooxidation of Gold Nanoparticles Coated with Alkanethiol Self-Assembled Monolayers. *J. Phys. Chem. C* **2021**, *125*, 2719-2728.
(51) Plieth, W. J. Electrochemical properties of small clusters of metal atoms and their role in the surface enhanced Raman scattering. *J. Phys. Chem.* **1982**, *86*, 3166-3170.
(52) Nanda, K. K.; Sahu, S. N.; Behera, S. N. Liquid-drop Model for the Size-dependent Melting of Low-dimensional Systems. *Phys. Rev. A* **2002**, *66*, 013208.
(53) Garzon, I. L.; Avalos Borja, M.; Blaisten-Barojas, E. Phenomenological Model of Melting in Lennard-Jones Clusters. *Phys. Rev. B* **1989**, *40*, 4749-4759.
(54) Rey, C.; Gallego, L. J.; Garcia-Rodeja, J.; Alonso, J. A.; Iniguez, M. P. Molecular-dynamics Study of the Binding Energy and Melting of Transition-metal Clusters. *Phys. Rev. B* **1993**, *48*, 8253-8262.
(55) Soule de Bas, B.; Ford, M. J.; Cortie, M. B. Melting in Small Gold Clusters: A Density Functional Molecular Dynamics Study. *J. Phys.-Condens. Mat.* **2006**, *18*, 55–74.
(56) Reich, M.; Utsunomiya, S.; Kesler, S. E.; Wang, L.; Ewing, R. C.; Becker, U. Thermal Behavior of Metal Nanoparticles in Geologic Materials. *Geology* **2006**, *34*, 1033-1036.
(57) Popescu, R.; Schneider, R.; Gerthsen, D.; Böttcher, A.; Löffler, D.; Weis, P.; Kappes, M. M. Coarsening of Mass-selected Au Clusters on Amorphous Carbon at Room Temperature. *Surf. Sci.* **2009**, *603*, 3119–3125.
(58) Nelli, D.; Rossi, G.; Wang, Z.; Palmer, R. E.; Ferrandod, R. Structure and Orientation Effects in the Coalescence of Au Clusters. *Nanoscale* **2020**, *12*, 7688-7699.
(59) Wan, Q.; Hu, S.; Dai, J.; Chen, C.; Li, W.-X. First-Principles Kinetic Study for Ostwald Ripening of Late Transition Metals on TiO2(110). *J. Phys. Chem. C,* **2019**, *123*, 1160−1169.
(60) Liu, Y.; Tsunoyama, H.; Akita, T.; Tsukuda, T. Size Effect of Silica-supported Gold Clusters in the Microwave-assisted Oxidation of Benzyl Alcohol with H2O2. *Chem. Lett.* **2010**, *39*, 159161.

TOC Figure

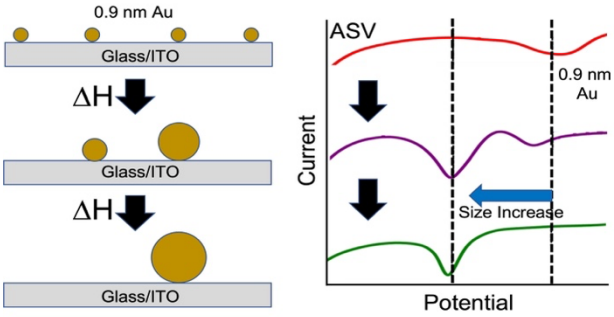
0.9 nm Au
Glass/ITO
ΔH
Glass/ITO
ΔH
Glass/ITO
ASV
0.9 nm Au
Current
Size Increase
Potential